



HAL
open science

Application of proton magnetic resonance soundings to groundwater reserve mapping in weathered basement rocks (Brittany, France)

Robert Wyns, Jean-Michel Baltassat, Anatoly Legchenko, Patrick Lachassagne, Jacques Vairon, Francis Mathieu

► To cite this version:

Robert Wyns, Jean-Michel Baltassat, Anatoly Legchenko, Patrick Lachassagne, Jacques Vairon, et al.. Application of proton magnetic resonance soundings to groundwater reserve mapping in weathered basement rocks (Brittany, France). Bulletin de la Société Géologique de France, 2004, 175 (1), pp.21-34. 10.2113/175.1.21 . hal-03783892

HAL Id: hal-03783892

<https://brgm.hal.science/hal-03783892v1>

Submitted on 22 Sep 2022

HAL is a multi-disciplinary open access archive for the deposit and dissemination of scientific research documents, whether they are published or not. The documents may come from teaching and research institutions in France or abroad, or from public or private research centers.

L'archive ouverte pluridisciplinaire **HAL**, est destinée au dépôt et à la diffusion de documents scientifiques de niveau recherche, publiés ou non, émanant des établissements d'enseignement et de recherche français ou étrangers, des laboratoires publics ou privés.

Application of proton magnetic resonance soundings to groundwater reserve mapping in weathered basement rocks (Brittany, France)

ROBERT WYNS¹, JEAN-MICHEL BALTASSAT², PATRICK LACHASSAGNE³, ANATOLY LEGCHENKO^{2,4}, JACQUES VAIRON¹ and FRANCIS MATHIEU²

Key words. – Nuclear magnetic resonance, NMR, Proton magnetic resonance, PMR, Surface nuclear magnetic resonance, Hydrogeology, Fissured zone, Hard rock aquifers, Weathering.

Abstract. – The Proton Magnetic Resonance (PMR) or Nuclear Magnetic Resonance (NMR) method, coupled with geometrical aquifer modelling, has been used to create a map of groundwater reserves over a 270 km² study area in a weathered basement setting. Most of the reserves are contained in a stratiform multi-layer aquifer whose geometry is influenced by the weathering front. The depths to the interfaces determined by PMR are considered and validated by comparison with the geometrical approach. Water contents and decay times of the PMR signal for each weathered layer are compared with the hydrogeological model. The results of the study show a decrease in water content from the top downwards for the three main aquifer layers (respectively : unconsolidated alterite, and an upper and a lower fissured zone). The groundwater reserves (80 % in the fissured zone and 20 % in unconsolidated alterite) represent approximately three years of average infiltration.

Utilisation des sondages de résonance magnétique protonique pour la cartographie de la réserve en eau souterraine en contexte de socle altéré (Bretagne, France)

Mots clés. – Résonance magnétique nucléaire, RMN, Résonance magnétique protonique, RMP, Hydrogéologie, Horizon fissuré, Aquifères de socle, Altération.

Résumé. – Les développements menés ces dernières années sur la méthode de Résonance Magnétique Protonique (RMP) ou Résonance Magnétique Nucléaire (RMN) ont débouché sur la mise au point d'un outil permettant la mesure non destructive depuis la surface du profil vertical de teneur en eau jusqu'à une profondeur de 50 à 100 m. Par ailleurs, les développements conceptuels nouveaux sur les propriétés hydromécaniques des socles altérés permettent une meilleure compréhension de la structure des aquifères de socle : il mettent en évidence la structure multicouche de la plupart de ces aquifères. La modélisation géométrique des horizons d'altération et de la surface piézométrique, couplée à des sondages de résonance magnétique protonique, a permis de réaliser pour la première fois une cartographie quantitative de la réserve en eau souterraine sur une région de 270 km² en contexte de socle altéré (Finistère nord). La profondeur des interfaces déduite des résultats d'inversion des sondages RMP a été validée par comparaison avec le modèle géométrique calculé à partir des données de forages. La teneur en eau et le temps de décroissance du signal RMP, lié à la taille des pores, ont été confrontés pour chaque horizon d'altération avec le modèle hydrogéologique. Les résultats de l'étude montrent une décroissance de la teneur en eau du sommet vers la base des horizons d'altération (respectivement : altérites, horizon fissuré supérieur et inférieur), dont l'épaisseur totale est de l'ordre 50 à 70 m. La réserve en eau souterraine, répartie à 80 % dans l'horizon fissuré et à 20 % dans les altérites meubles, représente approximativement trois ans d'infiltration moyenne.

INTRODUCTION

The quality of groundwater and surface water is increasingly threatened by the increasing use of fertilisers and pesticides in agriculture. In Brittany, this situation is worsened by the spreading of manure from intensive pig and poultry breeding. An increase in nitrate concentrations in groundwater and surface water threatens the drinking-water supply of the population. Furthermore, the transfer by streams of high quantities of nitrates into the sea causes each year, during the summer season, the onset of eutrophication of

coastal waters, which is detrimental to tourist activities and shellfish farming. In such a context, two of the key points involved in characterising the impact and durability of this diffuse pollution are an understanding (i) of the spatial distribution and quality of groundwater and (ii) of drainage processes involved in aquifer recharge.

The present study aims at testing the feasibility of quantitative mapping of groundwater reserves in basement domains by adopting a dual approach : (1) geometrical aquifer modelling based on drill-hole data, and (2) measuring water content in the different layers using proton magnetic reso-

¹ BRGM, Geology Department, Modelling and Applications Unit, BP 6009, 45060 Orléans cedex 2, France. r.wyns@brgm.fr

² BRGM, Land-Use Planning and Natural Hazards Department, BP 6009, 45060 Orléans cedex 2, France.

³ BRGM, Water Department, Water Resource Assessment and Discontinuous Aquifers Unit, 1039, rue de Pinville, 34000 Montpellier, France.

⁴ New adress: IRD, UR027, 32 av. H. Varagnat, 93143 Bondy cedex, France.

Manuscrit déposé le 14 janvier 2002 ; accepté après révision le 15 juillet 2003.

nance (PMR) soundings [Beauce *et al.*, 1996]. The study also aims at confirming recent conceptual developments concerning the understanding of the physical properties of weathered rocks [Wyns *et al.*, 1999], and to test the potential of the PMR method in such a context.

The present study forms part of a BRGM research project whose objective is to characterise variation laws of the physical properties of subsurface rocks (to a depth of 100 m) in order to establish maps and quantitative 3D models of these properties. Certain recent conceptual changes concerning the physical properties of weathered rocks, as presented in this article, directly evolve from the results acquired as part of this research project.

PROTON MAGNETIC RESONANCE SOUNDING METHOD

Until recently, no geophysical method could directly measure the *in situ* water content of geological formations. New developments in proton magnetic resonance (PMR), however, have made it possible to design non-destructive measuring devices that can record water contents from the surface [Beauce *et al.*, 1996 ; Gev *et al.*, 1996 ; Legchenko *et al.*, 1998]. We adopted the NUMIS device of Iris-Instruments.

To carry out a PMR sounding, a conductive antenna is laid out on the ground, generally in a circle with a diameter of 20 to 120 m, depending on the depth of the aquifer layers to be investigated. Different antenna geometries are incorporated into the Numis acquisition software, for example, the antenna can be laid out in a figure of eight that improves the signal-to-noise ratio [Trushkin *et al.*, 1994]. An alternating-current pulse is fed into the loop $i(t) = I_0 \cos(\omega_0 t)$, $0 < t \leq \tau$, I_0 and τ characterising respectively the amplitude and duration of the pulse. The emitted current pulse ω_0 corresponds to the Larmor frequency (noted f_0) of the protons within the geomagnetic field ω_0 , where H_0 is the amplitude of the geomagnetic field and γ the gyromagnetic factor of the protons (characteristic physical constant). Hence, the value of this frequency f_0 is deduced from the amplitude H_0 of the geomagnetic field at the considered site.

The current pulse causes a precession of the protons around the geomagnetic field, which in turn creates an alternating magnetic field that is detected, after switching off the injection current, by the same antenna as that used for transmission. In practice, the PMR response can only be recorded after an instrumental delay (known as 'dead-time') of 40 ms with the current version of Numis. The measurement acquisition process is shown on figure 1.

The PMR signal $e(t, q)$ describes an envelope of decreasing exponential shape $e(t, q) = E_0(q) \exp(-t/T_2^*) \cos(\omega_0 t + \varphi_0)$, where $E_0(q)$ is the initial PMR amplitude, T_2^* the spin-spin relaxation time, and φ_0 the phase of the PMR signal. $E_0(q)$, T_2^* and φ_0 are parameters measured by the receiver antenna. The sounding is performed by varying the excitation parameter $q = I_0 \tau$ that influences the depth of investigation. The three parameters $E_0(q)$, T_2^* and φ_0 are then interpreted to provide information concerning the water content at depth. The inversion algorithms of these PMR parameters are described in Legchenko and Shushakov [1998]. It should be noted that the detection of a PMR signal is directly related to the presence of water in the subsurface.

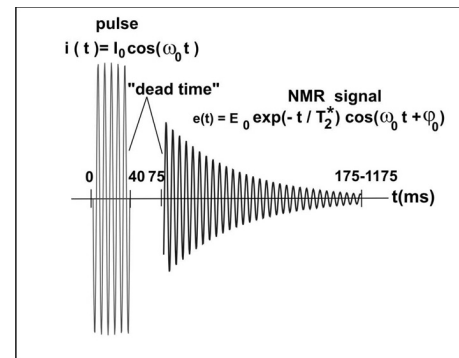


FIG. 1. – The Numis transmission-reception sequence as a function of time.

FIG. 1. – Séquence type émission-réception du dispositif Numis en fonction du temps.

When the signal is detected, further information can then be obtained from the recorded raw curves.

- The initial **amplitude** $E_0(q)$ is used to derive water-content variations with depth, and then the location and thickness of the aquifer. Amplitudes can vary from several tens of nanovolts to a few microvolts, depending on the water content of the considered environment. The Numis equipment has a detection threshold of about 4 nV. In unconfined aquifers, the depth to the top of the first water-bearing layer corresponds to the water table.

- The **decay time** T_2^* can be related to the average pore size in the aquifer formations, as indicated in table I. Considering the elements in table I, and the instrumental dead time required for switching the antenna from transmission to reception mode, a PMR response of water contained in clay ('bound', immobile water) cannot be detected by the current Numis equipment.

TABLE I. – Relationship between decay time and aquifer formation [from Shirov *et al.*, 1991].

TABL. I. – Relations entre le temps de décroissance T_2^* et la lithologie de quelques types d'aquifères [d'après Shirov *et al.*, 1991].

Decay time (ms)	Aquifer formation
<30	sandy clay
30 - 60	clayey sand, very fine sand
60 - 120	fine sand
120 - 180	medium sand
180 - 300	coarse and gravelly sand
300 - 600	gravel
600 - 1000	free water table

- The **phase** φ_0 provides information concerning the distribution of subsurface electrical conductivity, which influences the depth of investigation of a PMR sounding. Although this type of conductivity data is less precise than those supplied by traditional electrical methods, they must be taken into consideration during PMR data inversion for the accurate evaluation of depths to the various aquifers when resistivities are below 10 ohm-m.

The volume investigated during a sounding is defined as a vertical cylinder of a diameter approximately equal to 1.5 times the diameter of the loop, upon which it is centered,

and of a height equal to this diameter. For example, with a loop of 100 m in diameter, the maximum depth of investigation, if there is no highly conductive layer, is about 120 m. It takes two hours to perform a PMR sounding under favourable conditions (low parasite electromagnetic noise, whether of natural or anthropic origin).

Let us now examine what is the water content derived from the PMR sounding method. For an investigated volume V , let V_W be the part filled with water, and V_R be the part occupied by the solid phase ($V = V_W + V_R$). The water volume V_W may be split in into two parts : water in a homogeneous geomagnetic field, or 'free water' V_{free} , and water in an inhomogeneous geomagnetic field, or 'bound water' V_{bound} , thus $V_W = V_{free} + V_{bound}$. The response of bound water, which corresponds to a short decay time, cannot be measured by currently available equipment. Hence, the recorded PMR signal only corresponds to the part of the investigated volume occupied by free water : $n = V_{free}/V$. The two extreme cases are $n = 0\%$ (dry rock or compact clay) and $n = 100\%$ (bulk water in a lake). The quantitative correlation between free water detected by PMR and effective porosity used in hydrogeology depends on rock type. Consequently, an empirical calibration is generally required to increase the accuracy of the results.

GEOLOGY

The 270 km² study area is located north of Brest in the northern Finistère district in Brittany, France (fig. 2). It corresponds to the eastern part of the 1 : 50,000-scale Plabennec geological map [Outin *et al.*, 2001].

The area is underlain by Hercynian plutonic and metamorphic rocks (fig. 3), including granite, gneiss, mica schist and amphibolite. These rocks are capped on the plateaux by a thick weathered cover : outcrops of the solid bedrock are only observed in the deepest valleys. The weathered cover, which can be up to several tens of metres thick, was developed during long periods of continental weathering, probably during the first half of the Tertiary.

In the ancient metamorphic or plutonic basement, the rocks are generally massive with a low permeability. The presence of groundwater essentially depends on physical modifications undergone by these rock massifs after their formation, and particularly on their degree of fracturing and weathering.

Weathering generates an unconsolidated cover with variable porosity and permeability, depending on the mineralogy and texture of the parent rock. Beneath this unconsolidated cover, weathering also leads to *intense fissuring* that, where intersected by a drill hole, drains the overlying cover.

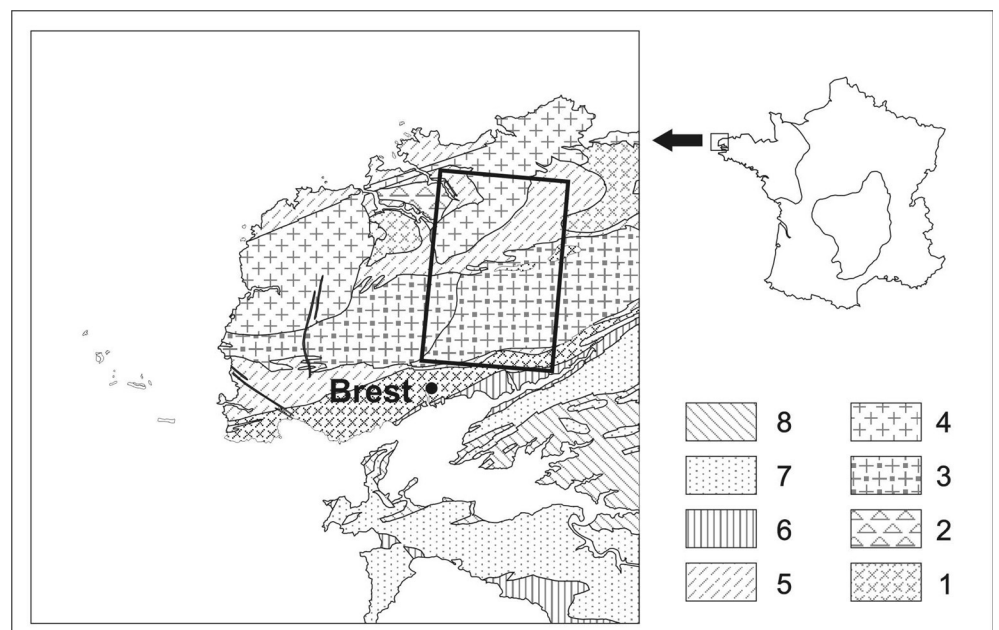
Tectonic fracturing induces water circulation if the fractures are open, as is the case with commonly subvertical fracture corridors where the degree of opening is related to i) their formation mechanism, and ii) their orientation with respect to the current stress field [Boeckh, 1992 ; Huntoon, 1986 ; Massonat, 1994]. Nevertheless, in the subsurface (less than a few hundred metres depth), the effect of anisotropic horizontal stress on the degree of fracture opening is disputed. This can be masked by other factors, such as an anisotropy of the original properties of the fractures, their connectivity and their clogging [Banks *et al.*, 1996], and by topographic effects [Burlet, 1991 ; Cornet and Burlet, 1992].

In the present study, however, only weathering and its associated fissuring are taken into consideration : both globally concern surfaces and, consequently, incomparably greater volumes than fracture corridors, which are localised systems.

In crystalline basement rocks, weathering leads to the formation of a cover of unconsolidated alterite (or saprolite), several tens of metres thick. At the scale of this work (several hundred square kilometres), the base of the alterite cover can be considered as sub-horizontal, parallel to the paleosurface contemporaneous with weathering (fig. 4). Weathering causes the dissolution and evacuation of the most soluble cations, depending on the nature and stability of the minerals to which they are bound, which in turn generates mineralogical phase changes, leading in par-

FIG. 2. – Location and geological setting of the study area. 1 : orthogneiss ; 2 : amphibolite ; 3 : aluminous monzogranite ; 4 : calc-alkaline and peraluminous granite ; 5 : gneiss and mica schist ; 6 : Proterozoic (Brioverian) schist ; 7 : Ordovician and Silurian rock ; 8 : Devonian rock.

FIG. 2. – Localisation et contexte géologique de la zone d'étude. 1 : orthogneiss ; 2 : amphibolite ; 3 : monzogranite alumineux ; 4 : granite calco-alcalin et peralumineux ; 5 : gneiss et micaschiste ; 6 : schiste briovérien ; 7 : Ordovicien et Dévonien ; 8 : Dévonien.



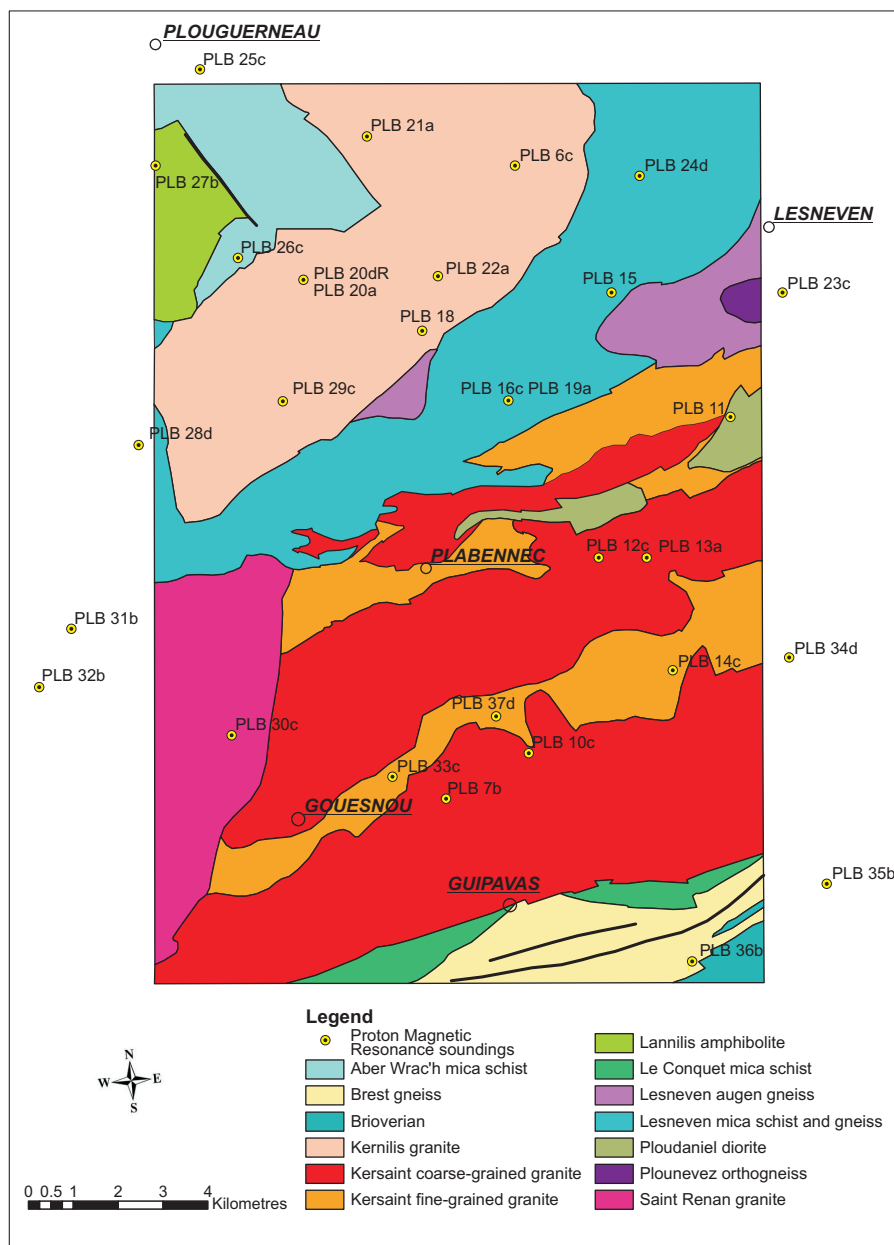


FIG. 3. – Map of the study area showing the geology and location of the Numis soundings.
 FIG. 3. – Carte géologique de la zone d'étude et localisation des sondages Numis.

ticular to the formation of clayey minerals at the expense of alumina silicates. Although alterite has an interstitial porosity, their clayey mineral content means that their permeability is generally low, especially in fine-grained rocks.

A fissured zone develops beneath the alterite, and is generally some 50 m thick in France. The fissuring results from rock shattering under the influence of stress generated by the swelling of certain minerals during the early stages of weathering [Wyns *et al.*, 1999]. The most sensitive mineral to swelling is biotite, which, at an early stage of weathering, transforms into chlorite before evolving into clayey minerals, meaning that the interfoliate space grows from 10 Å to 14 Å. Fissured zones thus preferentially develop in biotite-bearing rock. The density of weathering-related fissures decreases from the top downwards, becoming non-ex-

istent some 50 m beneath the weathering front. In foliate rock, weathering-related fissures show no clear orientation pattern. Conversely, in isotropic rock such as granite, the fissures have a sub-horizontal planar geometry (fig. 5); the spacing between fissures is some 10 cm at the top of the fissured zone and increases with depth. The hydrogeological properties of the fissured zone are characterised by a low porosity (< 5 %) of the fracture type, an overestimate of which can be gained, at least for granite, from the fissure geometry at outcrop (fig. 5). The global permeability of the fissured zone is generally higher than that of the alterite. Within the actual fissured zone, permeability decreases statistically with depth [Barker *et al.*, 1992; Davis and Turk, 1964; Detay *et al.*, 1989; Jones, 1985], in a similar way to fissure density.

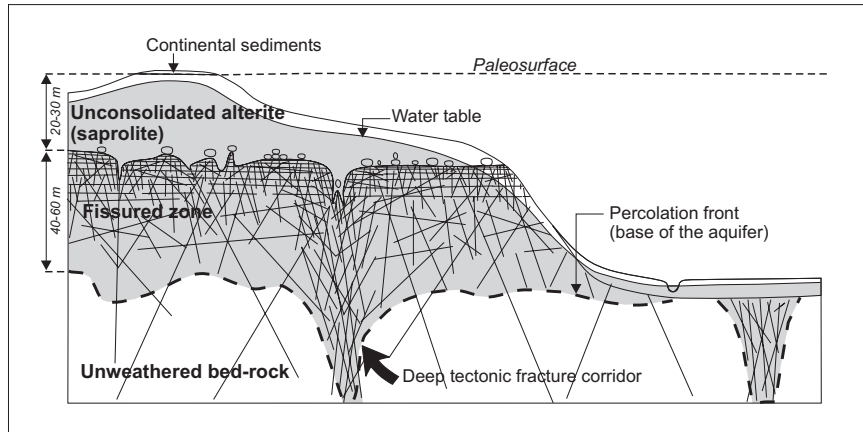


FIG. 4. – Conceptual model of hydrogeological properties in weathered basement rock.

FIG. 4. – *Modèle conceptuel des propriétés hydrogéologiques en contexte de socle altéré.*

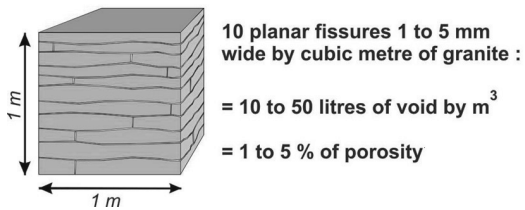


FIG. 5. – Photograph and theoretical porosity of a granite in the upper fissured zone

FIG. 5. – *Photographie et porosité théorique d'un granite dans la partie supérieure de l'horizon fissuré.*

Most hydrogeological frameworks of weathered crystalline massifs can be represented by a sub-horizontal two-layer system cut by vertical fractures of tectonic origin that act as drains :

- An upper layer is composed of unconsolidated alterite (20-30 m thick) that, considering its relatively high effective porosity, plays an essential storage role with respect to infiltrated rainwater. The water it contains is generally not directly exploitable by small-diameter drill holes due to its low permeability ;

- A lower layer, including the fissured zone (about 50 m thick), has a drainage role with respect to the overlying storage layer, at least at the scale of intersecting drill holes, as well as a significant storage role. It supplies in certain cases perennial springs that contribute to the minimum flow of the rivers ; this is the target layer of most drill holes put down into the basement and generally provides significant yields ($\leq 5 \text{ m}^3/\text{h}$) ;

- Vertical fractures of tectonic origin constitute, where sufficiently open, traditional targets for “high-flowrate” groundwater exploitation in this type of environment. They also drain water from the storage layer towards drill holes, in places via the fissured zone.

GEOMETRICAL MODELLING OF THE AQUIFER

We adopted a grid model with a 50-m cell size and corresponding to the digital elevation model (DEM) used.

In order to determine the amount of water contained in the stratiform aquifers, it is necessary beneath each line to define the thickness of the water-saturated column in each weathered layer. The first phase of work thus involved determining the geometry of the main interfaces (fig. 6) :

- The topographic ground surface is given by the National Geographic Institute DEM ;
- The water table was modelled using the DEM and some 40 calibration points derived from the few water-table measurements available.
- The base of the alterite was modelled by kriging drill-hole data derived from the “Banque de Données du Sous-Sol” (SubSurface dataBase : SSB) ;
- The base of the fissured zone was deduced from the PMR measurements ;

Base of the alterite

The study area has 225 drill holes that intersect the base of the alterite ; the geological logs of these drill holes are stored in the SSB. These data were complemented with out-crop observations, which allowed the elevation of this basal surface to be determined on the basis of 91 supplementary points. The elevation of the basal surface of the alterite was interpolated by kriging using all 316 points.

The contour map of the interface between the alterite and the underlying fissured zone is given on figure 7. The base of the alterite dips shallowly to the north, with some small-amplitude depressions associated with a stronger progression of the weathering front. It is offset in places by faults. Surface geometry is regular at the regional scale ; it represents a former weathering front probably gently dipping northward during the tectonic history and then incised

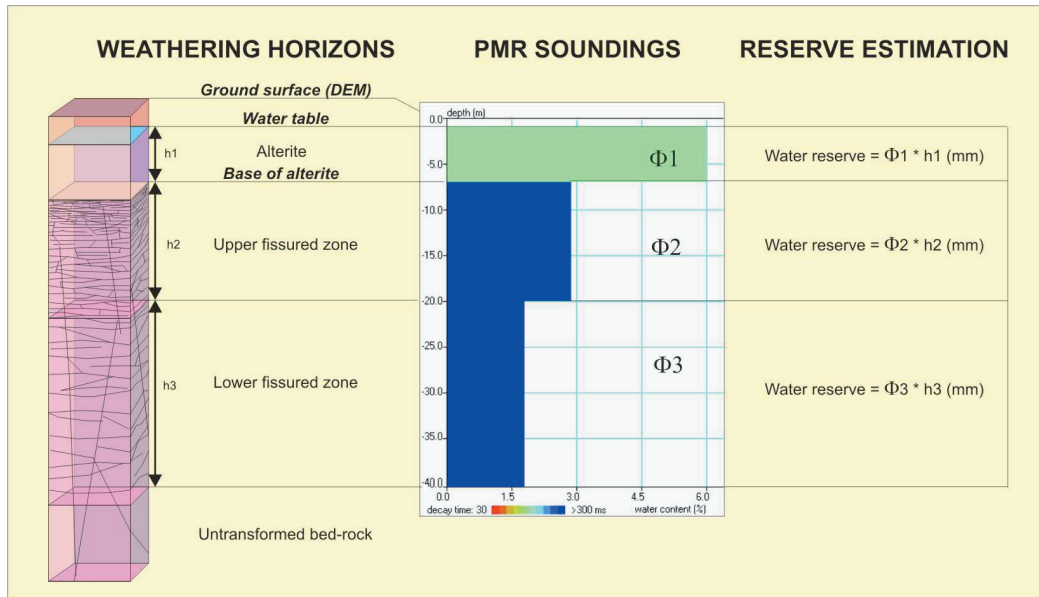
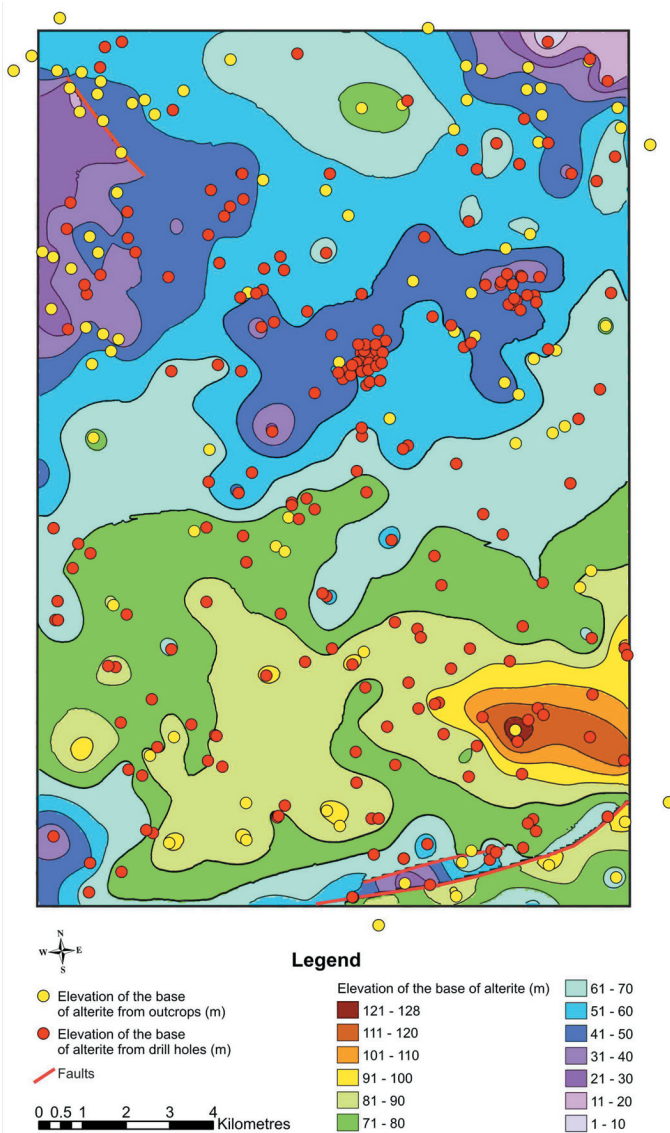


FIG. 6. – Stages involved in estimating the groundwater-reserve map.
 FIG. 6. – Schéma d'estimation de la réserve en eau souterraine.



during valley formation in the Quaternary. This regional regularity, validated by several similar studies [Wyns, 1991, 1998 ; Lachassagne *et al.*, 2001], disappears at outcrop scale where variations in elevation are of the order of several metres.

Water table

As the amount of available piezometric data was insufficient to establish a representative water-table map at the scale of the study area, we decided to geometrically model the water table.

In the context of the present study, where streams constitute groundwater outlets, the water table can be considered as being semi exposed in the thalweg bottoms of permanent streams. Considering the low permeability of the basement at catchment-basin scale, the water table rises significantly beneath the plateaux with increasing distance from the thalwegs. Most second- or third-order streams are thus perennial, meaning that the water table lies somewhere between the topographic surface and the envelope-surface of the base of the thalwegs (fig. 8).

The geometry of the envelope-surface of the thalweg base was modelled by kriging after automatic extraction of the drainage network using the DEM. Seventeen water-table measurement points were available over the study area ; for each point, we considered the ground and envelope-surface elevations for the thalweg base. For each measurement point, and according to the difference in elevation between the topographic surface and the basal thalweg surface ('a'

FIG. 7. – Elevation map of the base of the alterite derived from kriging of data from 225 drill holes (red circles) and 91 outcrop points (yellow circles)
 FIG. 7. – Carte isohypse de la base des altérites obtenue par krigeage à partir des données de forage (225 points, cercles rouges) et des observations de surface (91 points, cercles jaunes).

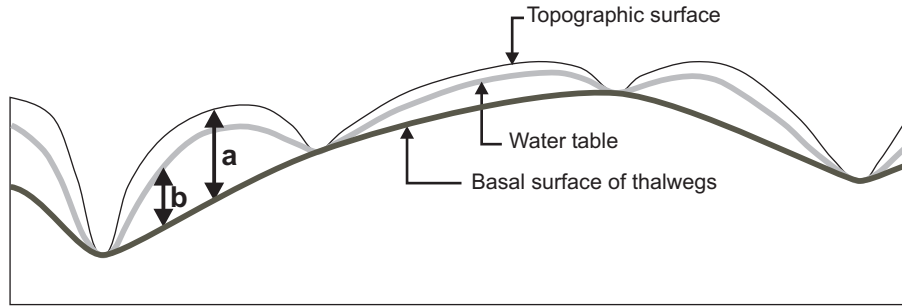


FIG. 8. – Principle of water-table modelling. a : difference of level between topographic surface and basal surface of thalwegs. b : difference of level between water table and basal surface of thalwegs.

FIG. 8. – Principe de modélisation de la surface piézométrique. a : dénivellation entre surface du sol et surface de base des thalwegs. b : dénivellation entre surface piézométrique et surface de base des thalwegs.

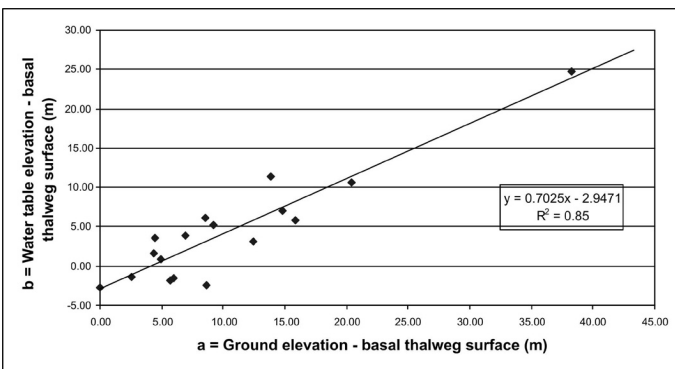


FIG. 9. – Relationship between water table, ground elevation and basal thalweg surface (17 piezometric readings from drill holes).

FIG. 9. – Relations entre surface piézométrique, altitude du sol et altitude de la surface de base des cours d'eau pérennes (17 mesures piézométriques réalisées en forages).

on fig. 8), we plotted the difference in elevation between the water table and the basal thalweg surface ('b' on fig. 8) on a binary diagram (fig. 9).

The measurement points form a linear trend described by the regression line of equation :

$$y = 0.7025 \cdot x - 2.9471 \quad [1]$$

with $R^2 = 0.85$

This equation allows us to calculate directly the elevation of the water table from the DEM and the elevation of the envelope-surface of the thalweg base. The negative y intercept (-2.95 m), which indicates that the water-table level is statistically located beneath the thalweg base level, may result from two factors : i) the thalwegs having been automatically extracted from the DEM, they may include both perennial and dry thalwegs ; ii) the water surface of the rivers generally is incised 1 m or more below the banks. The piezometric data calculated in this manner were used to control the geometrical coherence of the water tables measured by the Numis PMR soundings.

FIG. 11. – Measured versus calculated water table elevation from 44 piezometric readings (17 drill holes : ◆ and 27 Numis soundings : ⊙).

FIG. 11. – Comparaison entre piézométrie mesurée et piézométrie calculée (44 mesures piézométriques, dont 17 réalisées en forages : ◆ et 27 données Numis : ⊙).

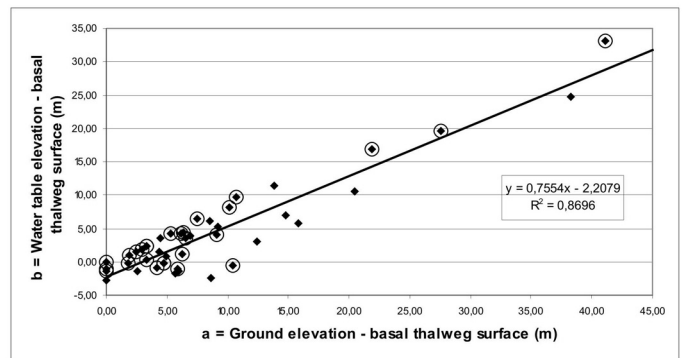


FIG. 10. – Relationship between water table, ground elevation, and basal thalweg surface (44 piezometric readings from 17 drill holes : ◆ and 27 Numis soundings : ⊙).

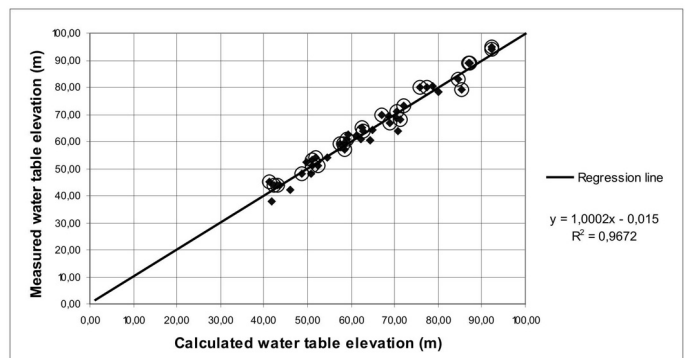
FIG. 10. – Relations entre surface piézométrique, altitude du sol et altitude de la surface de base des cours d'eau pérennes (44 mesures piézométriques, dont 17 réalisées en forages : ◆ et 27 données Numis : ⊙).

After using the previous data to confirm the water-table determination by Numis (cf. next section "PMR Data"), we combined the Numis data with the drill-hole data in order to better constrain the regression line [1]. This equation, determined from 44 experimental points, becomes (fig. 10) :

$$y = 0.7554 \cdot x - 2.2079 \quad [2]$$

with $R^2 = 0.8696$

A comparison between the measured water table and that calculated using equation [2] (fig. 11) gives a regression line with a slope = 1 and a correlation coefficient r^2 of



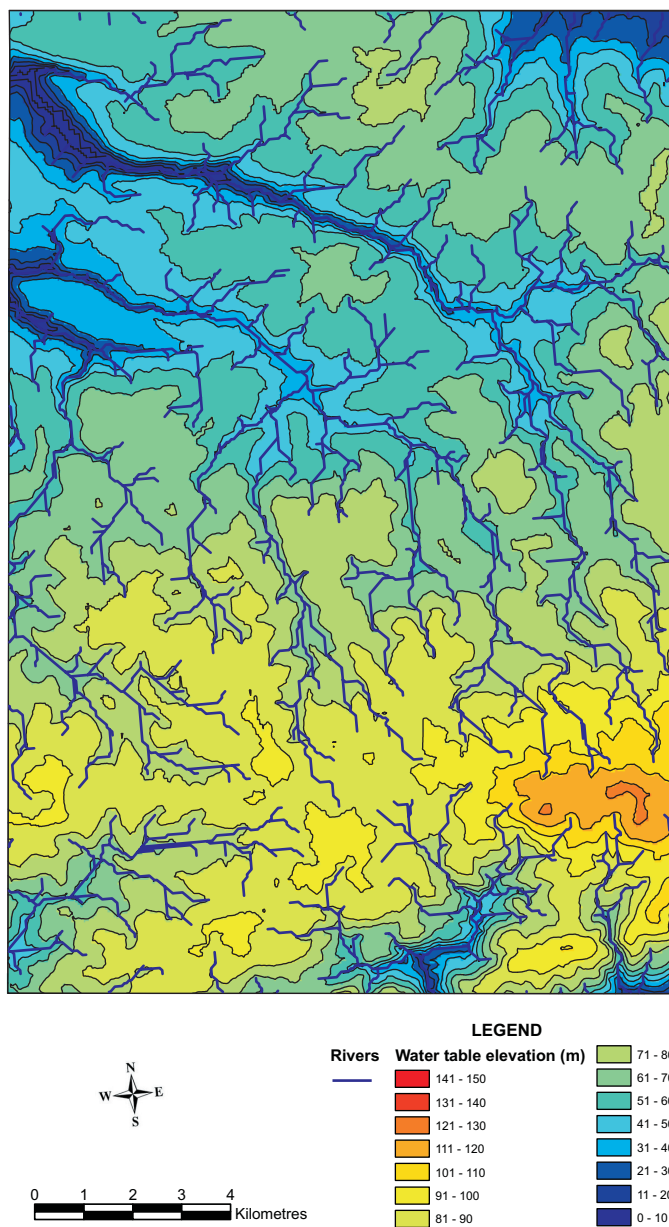


FIG. 12. – Water table elevation map modelled from DEM, elevation of the envelope-surface of the thalweg base and 44 water table measurements (equation [2]).

FIG. 12. – Carte de l'altitude de la surface piézométrique calculée à partir du MNT, de l'altitude de la surface de base des thalwegs, et de 44 points de mesures piézométriques (équation [2]).

0.967 ; the standard error is ± 2.67 m, and can be considered as reflecting the natural variability of the water table, because the water-table level measurements used are not synchronous.

The water table modelled with equation [2] is shown on figure 12. It has been used to determine the thickness of each weathered layer in the saturated zone.

Bull. Soc. géol. Fr., 2004, n° 1

Thickness of the fissured zone

For the fissured zone, the PMR soundings show, in agreement with the field observations and geophysical measurements carried out in a similar context [Wyns *et al.*, 1999], a decrease in the water content downwards. The inversion results generally enable to divide the fissured zone in an upper and a lower subzone, the former being characterised by higher water content and decay time than the latter. We estimated for each geological formation, the average thickness of the two parts of the fissured zone on the basis of the inversion results of the Numis soundings (table II).

Thickness of the layers in the saturated zone

The thickness of the alterite in the saturated zone was obtained by calculating the difference between the elevation of the water table and that of the basal alterite surface. The thickness of the fissured zone in the saturated zone was calculated in the same way.

PMR DATA

Data acquisition (table II)

The PMR measurements were carried out in three campaigns, June 1998, September 1998 and May 1999, using the Numis system of Iris-Instruments, complemented by a magnetometer and 600 m of injection and measurement cable. The purpose of these measurements was to determine, for each geological formation, the average vertical profile of water content in the weathered layers (alterite and fissured zone). Each campaign involved two people. The adopted antenna geometry, which significantly reduced the ambient electromagnetic noise, was a square figure-of-eight with sides 37 m long. The measurements were stacked between 50 and 300 times to improve the signal-to-noise ratio. A total of 30 soundings with recordings of satisfactory quality were performed.

Checking and geological interpretation of the inversion results

Each inversion diagram was compared against the geometrical modelling results of the interfaces so as to identify the nature of the weathered layer for each water content peak (unsaturated zone, alterite, fissured zone). This made it possible to check the coherence between the inversion results and the geometrical modelling results (table II).

Water table

Water-table elevations deduced from Numis soundings were compared (fig. 13) with those obtained through modelling drill-hole data (equation [1] and fig. 9). The error bar for the data derived from geometrical modelling was determined from the standard deviation of kriging residuals of the basal thalweg surface.

The regression line between Numis measurements and calculated values has a slope $\cong 1$ (1.03) and a correlation coefficient $r^2 = 0.975$. The ideal regression line, with a slope = 1 and a zero y-intercept, cuts the error bar of all the calculated values. The standard error is ± 2.52 m, which we can consider as reflecting natural water-table fluctuations.

TABLE II. – Numis acquisition parameters and geometrical controls of inversion results.
 TABL. II. – Paramètres d'acquisition Numis et contrôles géométriques des résultats d'inversion.

	COORDINATES (LAMBERT II EXTENDED)			ACQUISITION PARAMETERS AND INVERSION QUALITY				WATER-TABLE ELEVATION				BASAL SURFACE OF REGOLITH ELEVATION			THICKNESS OF FISSURED ZONE FROM NUMIS	
	X (m)	Y (m)	Ground elevation	Date	Antenna design	Stack number	Quality Index	From Numis	From geometrical modelling without Numis data (1)	From geometrical modelling with Numis data (2)	Kriging STD on modelling (+)	From Numis	From geometrical modelling	Kriging STD on modelling (+)	Upper fissured zone	Lower fissured zone
rnilis granite																
B 6c	103489	2419528	75.00	12/06/1998	Eight, 50 m	100	2.08	68.00	70.29	71.35	6.66	>68	74.91	8.55	17.00	36.00
B 18	100983	2416054	60.00	23/09/1998	Squ. eight, 37 m	200	2.43	59.00	56.48	57.32	5.55	56.00	55.91	6.41	12.00	44.00
PLB 20a	98602	2417320	54.00	24/09/1998	Squ. eight, 37 m	250	2.36	51.00	50.07	50.99	9.33	44.00	39.95	5.95		
B dR	98602	2417320	54.00	22/05/1999	Squ. Eight, 37 m	250	4.60	53.00	50.07	50.99	9.33	44.00	40.15	5.99		
PLB 21a	100239	2420492	62.00	25/09/1998	Squ. eight, 37 m	300	2.56	61.00	58.18	59.08	5.31	>61	61.98	10.72	14.00	46.00
PLB 22a	101628	2417176	46.00	25/09/1998	Squ. eight, 37 m	200	1.35	45.00	39.88	41.18	3.79	>46	56.50	10.16	17.50	10.00
PLB 29c	97983	2414805	46.00	21/05/1999	Squ. eight, 37 m	150	1.40	44.00	41.17	42.24	4.29	>46	51.50	10.85	14.50	51.00
rsaint coarse-grained granite																
B 7b	100633	2405632	90.00	15/09/1998	Eight, 50 m	50	1.75	89.00	86.06	86.97	13.48	83.00	82.73	11.53	13.00	40.00
PLB 10c	102609	2406483	90.00	17/09/1998	Squ. eight, 37 m	100	2.73	89.00	86.32	87.19	4.05	82.20	84.23	7.20	14.00	38.20
PLB 12c	104547	2410592	60.00	18/09/1998	Squ. eight, 37 m	200	2.90	59.00	57.18	57.90	2.47	>60	66.13	9.72	14.13	52.00
PLB 13a	105806	2410569	74.00	18/09/1998	Squ. eight, 37 m	200	1.26	72.00	67.78	69.10	5.25	>74	65.69	11.40	16.00	42.00
PLB 34d	108616	2408052	96.00	25/05/1999	Squ. eight, 37 m	150	1.58	94.00	91.22	92.29	5.14	78.00	84.62	10.39	10.00	
rsaint fine-grained granite																
PLB 14c	106006	2408002	87.00	19/09/1998	Squ. eight, 37 m	300	1.33	86.00	81.55	82.73	3.81	79.00	72.01	9.16		
PLB 33c	99560	2406219	97.00	24/05/1999	Squ. eight, 37 m	250	1.69	95.00	91.05	92.32	7.43	90.00	85.23	10.96		
PLB 37d	102032	2407328	88.00	26/05/1999	Squ. eight, 37 m	300	1.40	83.00	83.65	84.64	4.18	>83	86.96	5.51	17.00	38.00
int Renan granite																
PLB 30c	96045	2407471	90.00	21/05/1999	Squ. eight, 37 m	250	1.93	79.00	83.97	85.25	4.93	73.00	81.16	6.59	13.00	
PLB 31b	92679	2410129	81.00	22/05/1999	Squ. eight, 37 m	150	1.52	80.00	76.48	77.50	6.65	72.00	69.93	11.14		
PLB 32b	91843	2408935	73.00	24/05/1999	Squ. eight, 37 m	150	1.10	71.00	69.52	70.36	2.60	>73	77.03	11.38	15.03	49.00
Ploudaniel diorite																
B 11	107898	2413519	72.00	21/09/1998	Squ. eight, 37 m	350	2.38	67.00	67.82	68.78	4.58	64.00	66.98	10.18	6.00	46.00
ounevez orthogneiss																
PLB 23c	109186	2416152	71.00	18/05/1999	Squ. eight, 37 m	200	3.01	70.00	65.83	66.96	6.69	52.00	60.13	11.24		
nnilis amphibolite																
PLB 27b	95621	2420363	31.00	20/05/1999	Squ. eight, 37 m	250	0.98	27.00	20.67	22.72	5.59	>27	27.54	10.34	5.54	51.00
est gneiss																
PLB 35b	109009	2402987	81.00	25/05/1999	Squ. eight, 37 m	250	2.37	73.00	69.84	72.04	6.63	66.00	78.44	10.45		
PLB 36b	105919	2401536	88.00	26/05/1999	Squ. eight, 37 m	150	2.00	80.00	72.83	75.74	6.74	72.00	77.80	9.87		
sneven mica schist and gneiss																
B 15	105398	2416492	62.00	20/09/1998	Squ. eight, 37 m	200	1.91	57.00	57.64	58.63	4.28	48.00	56.00	8.99		
PLB 16c	103060	2414278	54.00	22/09/1998	Squ. eight, 37 m	250	2.81	54.00	51.05	51.79	0.00	50.00	47.42	4.76	10.00	46.00
PLB 19a	103060	2414278	65.00	24/09/1998	Squ. eight, 37 m	100	2.70	64.00	62.05	62.79	0.00	>65	66.29	12.10		
PLB 24d	106250	2419052	70.00	18/05/1999	Squ. eight, 37 m	200	2.18	65.00	60.56	62.45	6.88	56.00	56.59	8.10		
PLB 28d	94704	2414108	53.00	20/05/1999	Squ. eight, 37 m	200	1.84	48.00	47.34	48.56	4.53	42.00	45.45	11.33		
er Wrac'h mica schist																
PLB 25c	96644	2422278	56.00	19/05/1999	Squ. eight, 37 m	150	2.63	51.00	51.20	52.27	3.90	46.00	54.07	9.17	7.00	43.00
PLB 26c	97250	2418029	47.00	19/05/1999	Squ. eight, 37 m	250	4.79	44.00	42.12	43.20	4.71	39.00	42.07	5.82	6.00	46.00

Confidence level on water-table modelling	95%	90%	80%
(1) Error on water table without Numis data [size = 17]	+/- 5.90 m	+/- 4.95 m	+/- 3.86 m
(2) Error on water table with Numis data [size = 44]	+/- 4.35 m	+/- 3.65 m	+/- 2.84 m

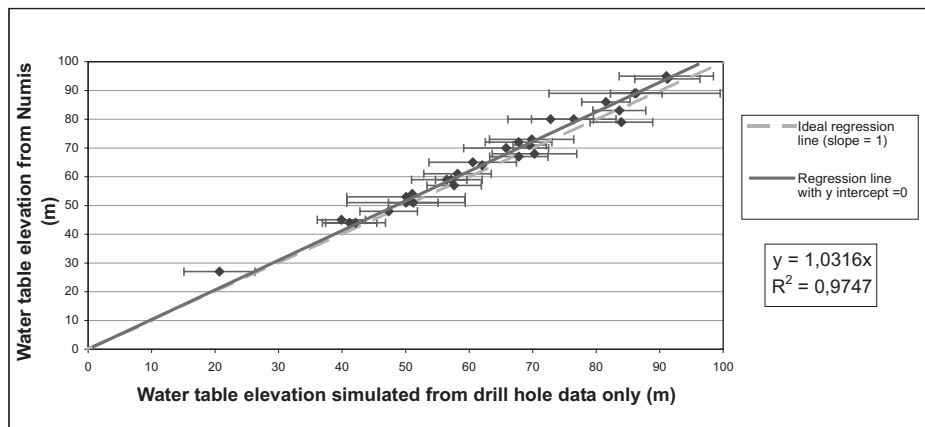


FIG. 13. – Comparison between measured water table elevation (Numis) and calculated water table elevation (drill holes). Error = kriging standard deviation of basal thalweg surface.
 FIG. 13. – Comparaison entre piézométrie déduite des mesures Numis et piézométrie calculée à partir des données de sondages seuls. Erreur = écart-type de krigeage de la surface de base des cours d'eau pérennes.

The available data indicate that the water-table level deduced from the Numis soundings is consistent with the geometrical modelling of piezometric level. Consequently, geometrical modelling of the water table carried out in conjunction with available water-table data and backed up by Numis soundings can be considered as reliable.

Base of the alterite

Among the 30 Numis soundings, 27 gave elevation values for the base of the alterite compatible with those determined through the geometrical modelling of drill-hole data, the differences falling within the standard deviation of kriging residuals (mean standard deviation : ± 7.5 m). The three other Numis soundings gave elevation values lower than the geometrical modelling results, with deviations of ± 3.5 m, taking into account the standard deviation of kriging residuals ; we relate these deviations to localised deepening of the alterite base. For the 20 Numis soundings that intersected the base of the alterite, a comparison between the elevation measured by Numis and that calculated through geometrical modelling (fig. 14) gives a regression line with a slope ≈ 1 (0.96), a y intercept = 0 and a correlation coefficient r^2 of

0.89. The ideal regression line (slope = 1, y intercept = 0) cuts the error bars of 19 out of the 20 kriged values. This deviation and the standard error of ± 5.38 m can be explained by the natural irregularity of the geometry of this interface. On the basis of the examined data, we can consider the elevation of the alterite base determined through Numis soundings to be significant.

DETERMINATION OF AVERAGE WATER CONTENT IN THE WEATHERED LAYERS OF EACH GEOLOGICAL FORMATION

Assuming that the physical properties resulting from supergene weathering vary vertically for the same lithology according to the difference in elevation with respect to the base of the alterite [Wyns *et al.*, 1999], we can try, for each geological formation, to characterise the average properties of each weathered layer from the Numis soundings. Where possible in terms of noise level, we attempted several Numis soundings for each geological formation (fig. 3) aiming at calculating average water contents for the alterite and the fissured zone. Among the 13 geological formations

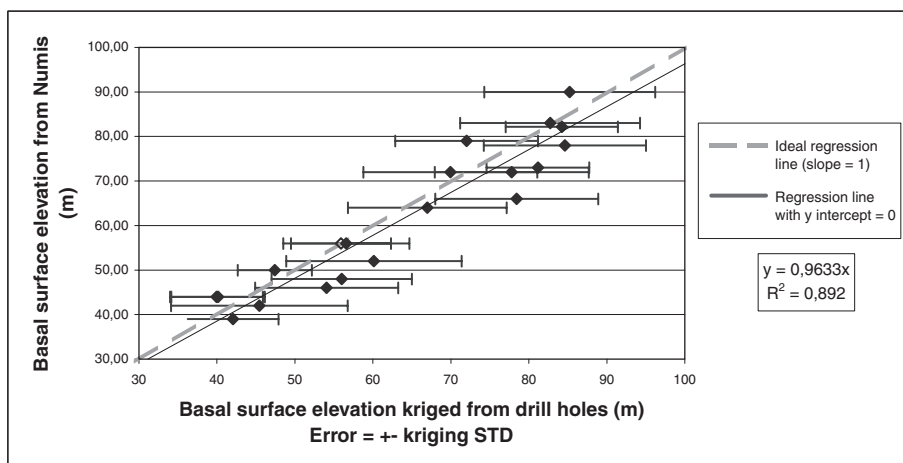


FIG. 14. – Comparison between basal alterite elevation measured by Numis and that obtained through kriging of drill-hole and field data. Error = kriging standard deviation of the base of the alterite.
 FIG. 14. – Comparaison entre l'altitude de la base des altérites déduite des mesures Numis et celle obtenue par krigeage des données de forages. Erreur = écart-type de krigeage de la surface de base des altérites.

identified in the study area, 10 have Numis soundings with exploitable results. It was not possible to investigate the other three formations (Lesneven augen gneiss, Conquet mica schist, Brioverian mica schist), underlying 13 km² of the entire 271 km².

Water contents

For each Numis sounding, the quality of recorded data can be characterised by the average signal-to-noise ratio, and the quality of inversion by the average fitting error (in %) between inverse model and measured data. These two parameters, which are calculated by the Numis data-processing software, are used to determine a quality index that can be used as a weighting factor for calculating the average water contents :

$$Q_s = S/N_s + (100-e_s)/100$$

where Q_s is the quality index of Numis sounding "s", S/N_s the average signal-to-noise ratio, and e_s the average fitting error.

The weighted mean of the water content for each horizon in each geological formation is obtained by the following calculation :

$$\tilde{W}_{h,g} = \frac{\sum (Q_s \times W_{h,s})}{\sum Q_s}$$

where $\tilde{W}_{h,g}$ is the weighted mean of water contents for each horizon of each geological formation, Q_s the quality index of Numis sounding "s", $W_{h,s}$ the raw water content obtained by inversion of a Numis sounding for one horizon in one sounding, h the weathering horizon, and g the geological formation.

The standard deviation of the weighted mean of water contents is obtained from the average of the deviation between raw water content and weighted water content :

$$Std(\tilde{W}_{h,g}) = \sqrt{\frac{\sum (W_{h,s} - \tilde{W}_{h,g})^2}{S}}$$

where $Std(\tilde{W}_{h,g})$ is the standard deviation of the weighted mean of water contents, and "n" the number of measurements.

The results show (table III), for each geological formation, a regular decrease in water content downward : 4-10 % in the alterite, 1-5 % in the upper fissured zone, and 0-3 % in the lower fissured zone. The less variable values are obtained for granites (alterite : 4.6-5.9 %, upper fissured zone : 1.6-4 %, lower fissured zone : 0.2-1.7 %), whereas schist, mica schist and gneiss give more variable values (alterite : 4.1-8.2 %, upper fissured zone : 0.6-6.1 %, lower fissured zone : 0-2.9 %). This decrease in water content downward is consistent with field and borehole observations, which show a decrease in the density of fissures and their degree of opening from the top of the fissured zone downwards. These relative variations also are consistent with literature data available for alterite [Acworth, 1987], also essentially relative. To our knowledge, no quantitative measurements of effective porosity are available in the literature for the fissured zone. The few measurements or estimates available for the alterite, whether direct through pumping tests (1-2 % [Compaore *et al.*, 1997]) or indirect through global reservoir modelling (Gardenia : 1-4 % [Thiery, 1987]) or meshed modelling (1-4.5 % [BRGM-AQUATER, 1991]), are similar to those obtained by PMR.

Decay time

For each geological formation, the weighted means of T2* and their standard deviations were calculated in the same way as the water contents. In seven cases out of nine, T2* increases significantly when passing from alterite (140 – 360 ms) into the upper fissured zone (240 – 1000 ms). This increase can be explained by a decrease in the signal-to-noise ratio associated with the fissured zone compared to the overlying weathered layer. The poor quality of the T2* determination for the deep part of the soundings, related to local noise conditions, means that it is impossible to discuss the interpretation of these values.

TABLE III. – Weighted mean water contents and T₂*. Data in italics correspond to individual measurements and not weighted means. Thicknesses with an asterisk relate to the entire fissured zone.

TABL. III. – Teneurs en eau et T₂* pondérés. Les valeurs en italiques correspondent à des mesures uniques et non à des moyennes pondérées. Les épaisseurs précédées d'une astérisque correspondent à l'ensemble de la zone fissurée.

	ALTERITE						UPPER FISSURED ZONE			LOWER FISSURED ZONE			
	Number of measurements	WATER CONTENT (%)		T2* (ms)		Number of measurements	WATER CONTENT (%)		Thickness retained from Numis	Number of measurements	WATER CONTENT (%)		Thickness retained from Numis
		Weighted mean	Standard deviation	Weighted mean	Standard deviation		Weighted mean	Standard deviation			Weighted mean	Standard deviation	
Kernilis granite	4	5.11	1.68	280.16	70.73	7	2.30	0.99	15.00	4	0.97	0.17	37.40
Coarse-grained Kersaint granite	2	4.65	0.42	360.75	148.16	3	4.04	0.56	13.43	3	1.70	0.24	43.05
Fine-grained Kersaint granite	2	5.09	3.65	308.60	15.41	3	1.60	1.17	15.00	1	1.60	-	40.35
Saint Renan granite	2	5.94	0.89	295.25	272.46	3	1.95	1.20	14.02	1	0.20	-	31.38
Ploudaniel diorite	1	9.59	-	143.60	-	1	4.96	-	6.00	1	0.73	-	46.00
Plounevez orthogneiss	1	4.52	-	307.60	-	1	0.09	-	*41.00	0	-	-	-
Lannilis amphibolite	0	-	-	-	-	1	0.40	-	5.54	1	0.13	-	51.00
Brest gneiss	2	8.25	3.47	87.79	22.33	2	0.61	0.30	*27.00	0	-	-	-
Lesneven mica schist and gneiss	4	4.11	1.76	210.32	58.81	5	1.90	1.73	10.00	1	0.00	-	37.35
Aber Wrac'h mica schist	2	7.98	1.10	330.84	82.77	2	6.15	0.29	6.50	2	2.91	1.47	44.50

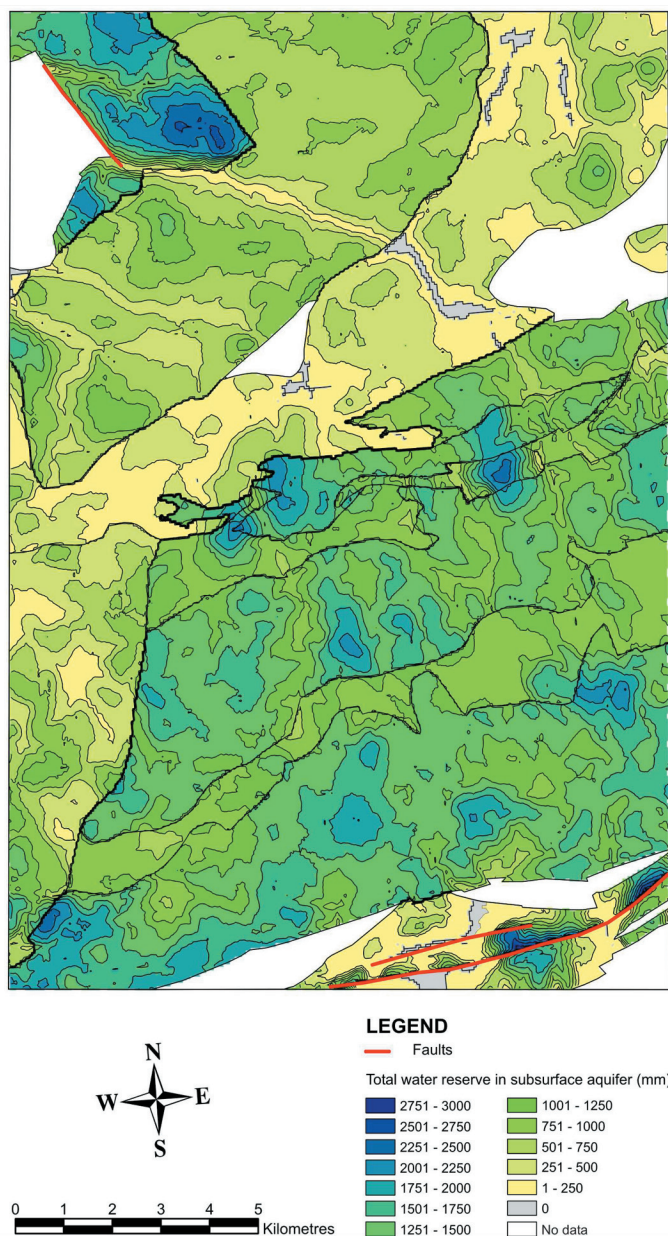


FIG. 15. – Thickness map of total groundwater reserve (in mm) in the weathered-rock aquifers.

FIG. 15. – Carte de la réserve en eau souterraine (exprimée en mm) contenue dans les horizons d'altération.

DISCUSSION

A map of water reserve (expressed in mm) contained in each weathered horizon was calculated for each of the three weathered layers (alterite, and upper and lower fissured zones). The sum of all three layers, representing the thickness of total water reserves in the aquifer, is presented on figure 15. This map shows significant contrasts in water reserve between geological formations, illustrating the degree of control exercised by lithology on the physical properties of the medium, in this case porosity.

Bull. Soc. géol. Fr., 2004, n° 1

The integration of water volumes per surface unit over 253 km² of the study area (some geological formations of the total 271 km² could not be investigated as explained before) is used to calculate the average thickness of water reserves stored in the aquifer : this is of the order of 960 mm for the fissured zone plus the alterite. Most reserves are located in the fissured zone (775 mm, i.e. 80 %), with the alterite only containing 185 mm (20 %). This is mainly due to the better preservation of the fissured zone, the alterite being more widely eroded, but also to the geometry of the water table with respect to the weathered layers ; actually, for 35 % of the study area, the elevation of the water table is below the bottom of the alterite. From another point of view, over 65 % of the study area, the elevation of the water table is above the bottom of the alterite, which indicates that recharge is largely controlled by the properties of the alterite.

The average value of efficient rainfall over the study area is about 500 mm [Louvrier and Margat, 1983 : annual averages for 1946-1976 ; Daum *et al.*, 1996 : annual averages for 1965-1994). Assuming a runoff between 25 % and 50 % of efficient rainfall, then annual infiltration can be estimated between 250 and 375 mm. Global modelling with the Gardenia software developed by BRGM [Boisson and Thiery, 1991 ; Thiery, 1988] was carried out for a well documented, 90 km² catchment basin and with a geology and a morphology similar to the study area (the Horn Basin in the Finistère Département of Brittany) [BRGM, 1999]. This made it possible to estimate what portions of the efficient rainfall contribute respectively to runoff and to infiltration ; the infiltrated part represents 297 mm, which is similar to, and thus confirms, the previous figure.

The thickness of water reserves in the weathered aquifers determined during the present study would thus represent approximately three years of average infiltration.

CONCLUSIONS

The present study had three main objectives : i) confirm the new conceptual model of stratiform aquifers in a weathered basement setting ; ii) test the possibilities of the PMR tool in such a context ; iii) map the spatial distribution of groundwater reserves in the aim of predicting and managing long-term groundwater quality.

Results concerning the structure and properties of the fissured basement aquifers

On the basis of some 30 PMR soundings distributed over about 270 km² and, bar a few exceptions, made away from the main fracture corridors, we obtained a representative sampling of the average geometry of the aquifers in this weathered basement region. Study of the inversion results of the Numis soundings shows that water contents are distributed according to a geometrical three-layer model with downward decreasing water contents. The calibration of these layers in relation to the geometrical model of the weathered horizons deduced from drill-hole data shows that the three layers correspond respectively to i) alterite, ii) an upper fissured zone, and iii) a lower fissured zone. The alterite is characterised by the highest water contents. The upper fissured zone has lower water contents than the alterite, and the lower fissured zone has the lowest water

TABLE IV. – Comparison between water contents from Numis (present study) and theoretical effective porosity [from Bodelle and Margat, 1980] for the different lithologies studied.

TABLE IV. – Comparaison entre les teneurs en eau obtenues par Numis (présente étude) et la porosité efficace théorique [d'après Bodelle et Margat, 1980] pour les différentes lithologies étudiées.

Lithology	Numis data	Effective porosity [Bodelle and Margat, 1980]
Granitic alterite	5 - 10%	1 - 10%
Fissured granite	0.2 - 5%	-
Schist alterite	4 - 8%	1 - 10%
Fissured schist	0.1 - 6%	0.5 - 5%

contents, compatible with a decrease in fissure density. This study confirms the new conceptual model for basement aquifers characterised by an aquifer unit composed of superimposed stratiform layers, cut by tectonic fracture corridors that locally serve as drains.

Results concerning validation of the PMR tool

In a context of sub-horizontal stratiform aquifers, the Numis instrument provides three types of information : i) geometrical data (depth to interfaces), ii) water-content data, and iii) decay-time data, related to pore size.

i) The geometrical position of the geological interfaces as derived from Numis data inversion was compared to that determined through kriging using drill-hole data. A total of 19 out of 20 of the Numis determinations falls within the kriging bracket of uncertainty. Similarly, the water table elevation as determined by Numis falls within the bracket of uncertainty for the water table as determined by modelling drill-hole data. We thus conclude that vertical calibration of the interfaces obtained through Numis data inversion is satisfactory, at least for the depth of investigation imposed by the adopted antenna geometry (i.e. – 40 m to – 50 m).

ii) According to the theory of nuclear magnetic resonance, the water contents measured by Numis correspond to contents of free water as opposed to water bound to the grains [Beauce *et al.*, 1996 ; Legchenko and Shusharov, 1998 ; Legchenko *et al.*, 1998 ; Shirov *et al.*, 1991]. The water contents determined by Numis can only be indirectly compared with true water contents, considering the large volume of rock involved. It is noted that the water contents recorded by Numis are, as expected, much lower than total porosity and relatively similar to effective porosity (table IV).

iii) The decay time $T2^*$ is, in theory, proportional to pore size. The experience acquired suggests that the results of decay-time measurements are sufficiently reliable for the alterite. For the fissured zone, the signal-to-noise ratio is unfavourable and in most cases the results of $T2^*$ measurements cannot be analysed. At present, we do not have the means to calibrate the $T2^*$ values with respect to the known parameters in this type of environment, even for the weathered zone. We could try and do this using drill-hole permeability data, between packers [Howard *et al.*, 1992] or with a borehole flowmeter.

Results concerning the feasibility of mapping groundwater reserves

A better knowledge of the spatial distribution of reserves is only of limited interest for groundwater development as it gives no indication about the value of the renewable resource or the exploitable flowrates. It nevertheless holds a certain value for establishing a water protection and management policy.

The motivation behind this mapping exercise is also related to an improvement of our understanding of the structure and functioning of weathered basement aquifers. Such a mapping approach provides quantitative data (particularly geometrical) that could constitute basic parameters for mathematical hydrogeological models representing the functioning of catchment basins. This approach should lead to more accurate estimation of residence times and mixing laws for groundwater stored in the various compartments of basement aquifers, and to better quantification of water-rock interactions, particularly for natural denitrification processes. The key points that remain to be solved include determination of the hydrodynamical parameters and drainage processes within these various compartments, at the watershed and catchment-basin scales.

The present study demonstrates the feasibility of quantitative mapping of groundwater reserves within different weathered aquifers. It has provided new data concerning the structure of these aquifers in the study area. Due to the intense erosion of the alterite, 80 % of the groundwater reserves is contained in the fissured zone, compared to only 20 % in the alterite. It must be borne in mind that fractures of tectonic origin are not taken into consideration in this study as their reserves are insignificant compared to those of weathering-related fissures. The average thickness of water reserves contained in the alterite (185 mm) is slightly lower than the average annual infiltration (250-375 mm). The average thickness of total reserves, calculated for the entire study area, represents about three years of infiltration.

A geometrical approach of the weathered aquifers, combined with quantification of water contents using nuclear magnetic resonance, can lead to a 3D representation of the effective porosity of these aquifers. The porosity deduced from PMR measurements still needs to be calibrated, by pumping tests for example. The second essential parameter for quantifying aquifer properties is permeability and, more specifically, connectivity properties at watershed or catchment-basin scale. Only a multi-disciplinary approach (drill-hole observations, pumping tests, water-table monitoring, geochemistry, etc.) could provide us with this parameter at such a scale. After methodological developments, PMR could contribute to filling this gap by improved interpretation and use of measured decay times.

Acknowledgements. – This study was co-financed by the County Council of Brittany, the Regional Council of Finistère, the Loire-Brittany Water Authority, the Ministry of Industry (BRGM Public Service grant) and the Ministry of Research (BRGM R&D project “3D mapping of parameters”). The authors would like to thank Rowena Stead and Marinus Kluijver of the BRGM Translation Department for translating the original French text, and Ghislain de Marsily and Henri Robain for improving the original text.

References

- ACWORTH R.I. (1987). – The development of crystalline basement aquifers in a tropical environment. – *Q. J. Eng. Geol.*, **20**, 265-272.
- BANKS D., ODLING N.E., SKARPHAGEN H., & ROHR-TORP E. (1996). – Permeability and stress in crystalline rocks. – *Terra Nova*, **8**, 223-235.
- BARKER R.D., WHITE C.C. & HOUSTON J.F.T. (1992). – Borehole siting in an African accelerated drought relief project. In : E.P. and B. WRIGHT, E.G., Eds., Hydrogeology of crystalline basement aquifers in Africa. – *Geol. Soc. Amer. Spec. Publ.*, **66**, 183-201.
- BEAUCE A., BERNARD J., LEGCHENKO A. & VALLA P. (1996). – Une nouvelle méthode géophysique pour les études hydrogéologiques : l'application de la résonance magnétique nucléaire. – *Hydrogéologie*, **1**, pp. 71-77, Orléans.
- BODELLE J. & MARGAT J. (1980). – L'eau souterraine en France. – Masson, Paris, 208 p.
- BOECKH E. (1992). – An exploration strategy for higher yield boreholes in the West African crystalline basement. In : E.P. and B. WRIGHT, E.G., Eds., Hydrogeology of crystalline basement aquifers in Africa. – *Geol. Soc. Amer. Spec. Publ.*, **66**, 87-100.
- BOISSON M. & THIERY D. (1991). – Logiciel Gardénia. Modèle Global A Réservoirs pour la simulation des DEbits et des Niveaux Aquifères. – BRGM, Orléans
- BRGM-AQUATER (1991). – Exploitation des eaux souterraines en socle cristallin et valorisation agricole : pilote expérimental en milieu rural pour des zones soudano-sahéliennes et sahéliennes. – BRGM-AQUATER, Orléans.
- BRGM (1999). – Qualité des eaux en Bretagne : ruissellement, infiltration, temps de réponse ; bassins versants : le Yar (Côtes d'Armor), l'Horn (Finistère), le Coët Dan (Morbihan). – Rapport BRGM R 40764, 62 p.
- BURLET D. (1991). – Détermination du champ de contraintes régional à partir de tests hydrauliques en forage : résultats de 9 expérimentations in-situ réalisées en France. – Ph.D. thesis, University of Paris VII, Paris, 260 p.
- COMPAORE G., LACHASSAGNE P., POINTET T. & TRAVI Y. (1997). – Evaluation du stock d'eau des altérites. Expérimentation sur le site granitique de Sanon (Burkina-Faso). – *Rabat IAHS conference*, IAHS, **241**, 37-46.
- CORNET F.H. & BURLET D. (1992). – Stress field determinations in France by hydraulic tests in boreholes. – *J. Geophys. Res.*, **97 B8**, 11829-11849.
- DAUM J.R., DESPRATS J.F. & DURAND F. (1996). – Précipitations efficaces moyennes annuelles en France (1965-1994). – Rapport BRGM R38975, 17 p., 4 annexes.
- DAVIS S.N. & TURK L.J. (1964). – Optimum depth of wells in crystalline rocks. – *Groundwater* **2**, 2, 6-11.
- DETAY M., POYET P., EMSSELLEM Y., BERNARDI A. & AUBRAC G. (1989). – Influence du développement du réservoir capacitif d'altérites et de son état de saturation sur les caractéristiques hydrodynamiques de forages en zone de socle cristallin. Development of the saprolite reservoir and its saturation state ; influence on the hydrodynamic characteristics of drillings in a crystalline basement. – *C. R. Acad. Sci.*, Paris II, **309**, 429-436.
- GEV I., GOLDMAN M., RABINOVICH B., RABINOVICH M. & ISSAR A. (1996). – Detection of the level in fractured phreatic aquifers using nuclear magnetic resonance (NMR) geophysical measurements. – *Jour. Appl. Geophys.*, **34**, 277-282.
- HOWARD K.W.F., HUGHES M., CHARLESWORTH D.L. & NGOBI G. (1992). – Hydrogeologic evaluation of fracture permeability in crystalline basement aquifers of Uganda. – *Hydrogeology J.*, **1**, 55-65.
- HUNTOON P.W. (1986). – Incredible tale of Texasgulf well 7 and fracture permeability, Paradox Basin, Utah. – *Groundwater* **24**, **5**, 643-653.
- JONES J. (1985). – The weathered zone aquifers of the basement complex areas of Africa. – *Q. J. Eng. Geol.*, **18**, 35-46.
- LACHASSAGNE P., PINAULT J.-L. & LAPORTE P. (2001). – Radon-222 emanometry : a relevant methodology for water well siting in hard rock aquifers. – *Water Resour. Res.*, **37**, 12, 3131-3146.
- LACHASSAGNE P., BÉRARD P., BRUEL T., CHÉRY L., COUTAND T., DESPRATS J.-F., LE STRAT P. & WYNS R. (2001). – Exploitation of high-yield wells in hard-rock aquifers. Downscaling methodology combining GIS and multicriteria analysis to delineate favourable zones. – *Groundwater*, **39**, 4, 568-581.
- LEGCHENKO A. & SHUSHAKOV O. (1998). – Inversion of surface NMR data. – *Geophysics*, **63**, 1, 75-84.
- LEGCHENKO A.V., BALTASSAT J.M., BEAUCE A., MAKKI M.A. & AL-GAYDI B.A. (1998). – Application of the surface proton magnetic resonance method for the detection of fractured granite aquifers. – *Proceedings of the IV Meeting of the Environmental and Engineering Geophysical Society (European Section)*, September 14-17, 1998, Barcelona (Spain), 163-166.
- LOUVRIER M. & MARGAT J. (1983). – Précipitations efficaces moyennes annuelles en France (1946-1976) ; carte à 1/1 500 000. – Rapport BRGM 83 SGN 003 EAU, Orléans.
- MABEE S.B. (1999). – Factors influencing well productivity in glaciated metamorphic rocks, Georgetown, Maine. – *Groundwater*, **37**, 1, 88-97.
- MASSONAT G. (1994). – Les réservoirs fissurés : modélisation de structures et simulation d'écoulements. – *Bull. Centres Rech. Expl.-Prod. Elf Aquitaine*, **18**, 1, 135-314.
- OUTIN J.M., THOMAS E., QUÉTÉ Y., BALLEVRE M., WYNS R. & GUENNOC P. (2001). – Carte géologique de la France à 1/50 000, feuille Plabennec n°238, et notice explicative. – BRGM, Orléans.
- SHIROV M., LEGCHENKO A. & CREER G. (1991). – New direct non-invasive ground water detection technology for Australia. – *Expl. Geophys.*, **22**, 333-338.
- THIERY D. (1987). – Analysis of long-duration piezometric records from Burkina Faso used to determine aquifer recharge. – *NATO advanced research workshop on estimation of natural recharge of groundwater*, I. SIMMERS Ed., Antalya. – Reidel Publishing Company, 477-489.
- THIERY D. (1988). – Forecast of changes in piezometric levels by a lumped hydrological model. – *J. Hydrology*, **97**, 129-148.
- TRUSHKIN D.V., SHUSHAKOV O.A. & LEGCHENKO A.V. (1994). – The potential of a noise-reducing antenna for surface NMR ground water surveys in the earth's magnetic field. – *Geophys. Prosp.*, **42**, 855-862.
- WYNS R. (1991). – Evolution tectonique du bâti armoricain oriental au Cénozoïque d'après l'analyse des paléosurfaces continentales et des formations géologiques associées. – *Géol. France*, **3**, 11-42.
- WYNS R. (1998). – Modélisation de la géométrie (altitude, épaisseur) des arènes granitiques du bassin-versant lozérien de la Truyère (Lozère, Massif central). – Rapport BRGM R 40191, 18 p., 9 fig., 4 pl. h.t.
- WYNS R., GOURRY J.-C., BALTASSAT J.-M. & LEBERT F. (1999). – Caractérisation multiparamètres des horizons de subsurface (0-100 m) en contexte de socle altéré. *2ème Colloque GEOFCAN*, BRGM, IRD, UPMC, pp. 105-110. Orléans, France.